Supporting Information

Droplet Microfluidics-Assisted Fabrication of Fe-Alginate Microgels with Complex Morphology: Effect of the Compositions of Droplets

Jie Chen [a], Penghui Li [a], Ran An [a], Aishan Cai [a], Kaiqi Wang [a], Zheyu Zhang [a], Tao Wang [e,*], Yuandu Hu [a, b, c, d,*]

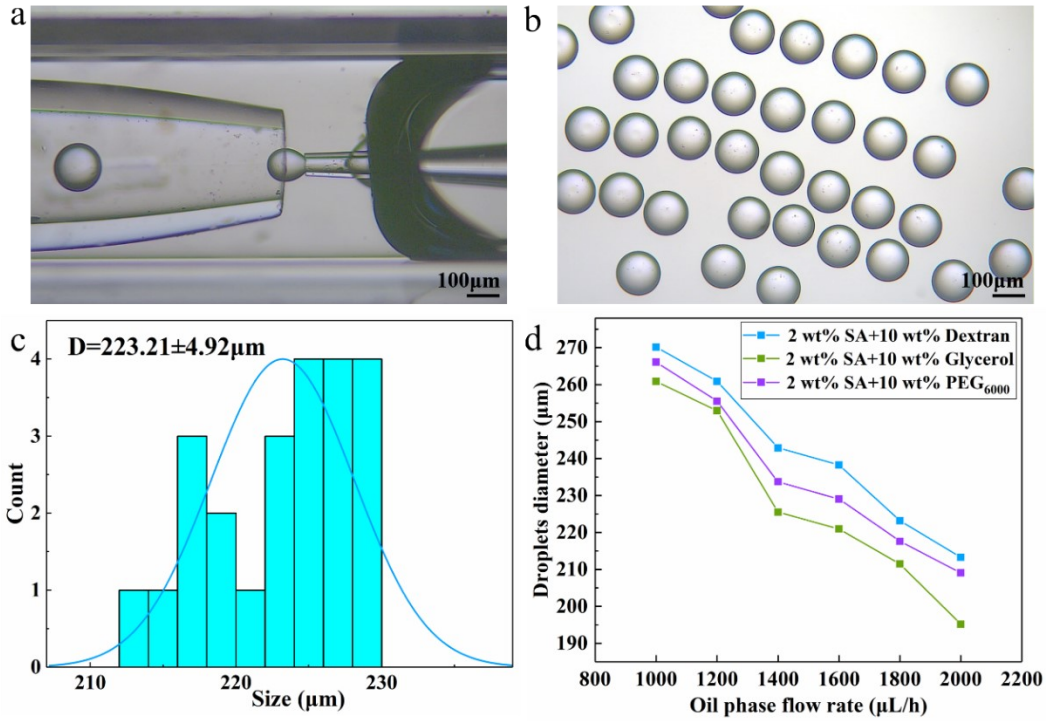

Figure S1. Figure S1. a. Optical microscopy image showing the generation of W/O droplets through the shear force of the CP in a microfluidic device. b. Optical microscopy image of the initial, non-crosslinked droplets produced from microfluidics. c: Statistical size distribution chart of the initial droplets generated from the microfluidic device and the chart indicated that the droplets with an average droplet size of ~ 223 μm. d: Size variation of initial droplets formed from SA solutions with

three different compositions by varying CP flow rates, while keeping the DP flow rate unchanged.

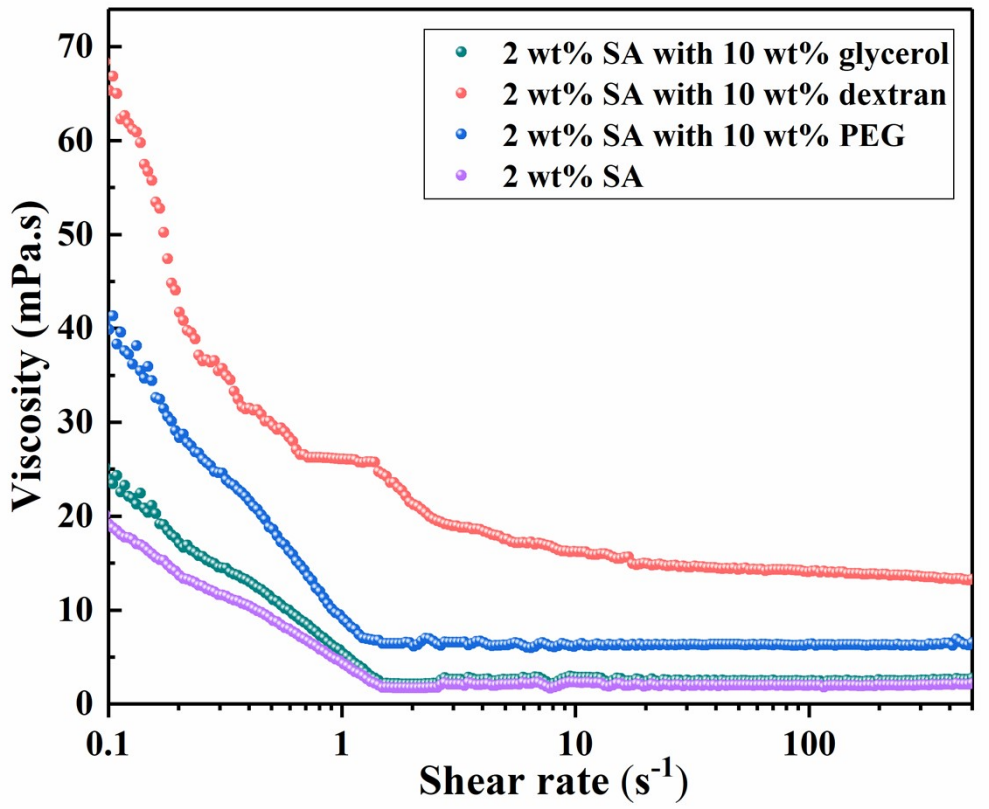

Figure S2. Shear rate-viscosity curves are obtained for three types of DP solutions, each consisting of 2 wt% SA and 10 wt% of any of the following three components: dextran (MW = 500,000), PEG (MW = 6,000), or glycerol (MW = 92).

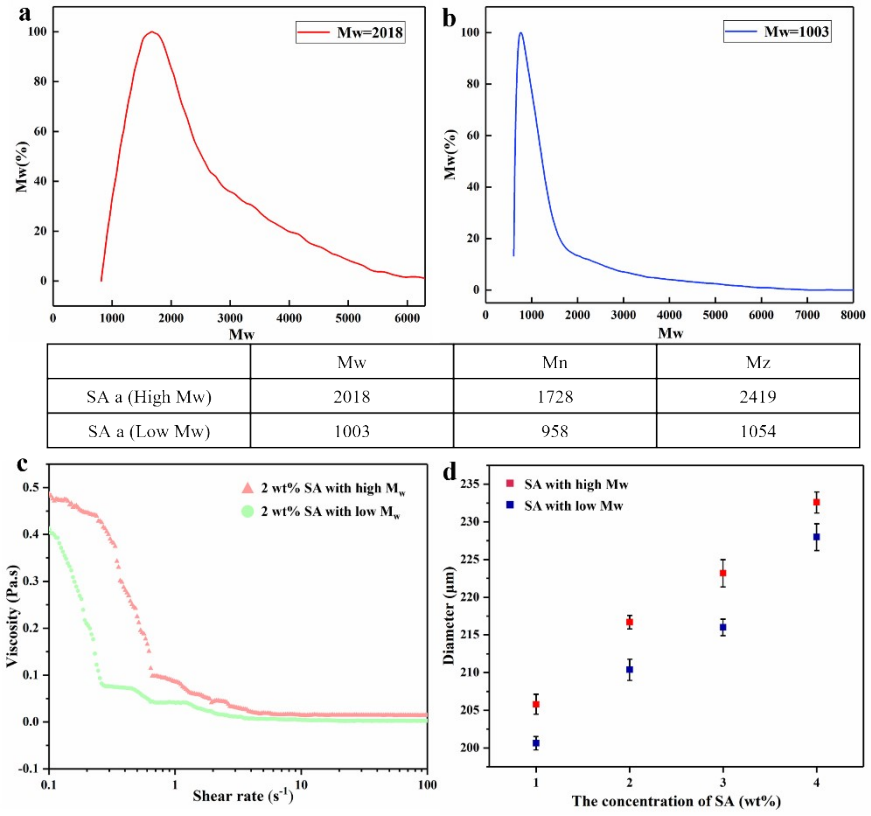

	Mw	Mn	Mz
SA a (High Mw)	2018	1728	2419
SA a (Low Mw)	1003	958	1054

Figure S3. a-b. Molecular weight distribution curves of SA with two different Mw. Table shows the detailed infotmation of the molecular weights and PDI. c. Shear rate-viscosity curves of two SA solutions with low and high molecular weights. d. Size variation of droplets produced by four SA solutions with different molecular weights at the same flow rate (DP=70 μL/h, CP=1200 μL/h).

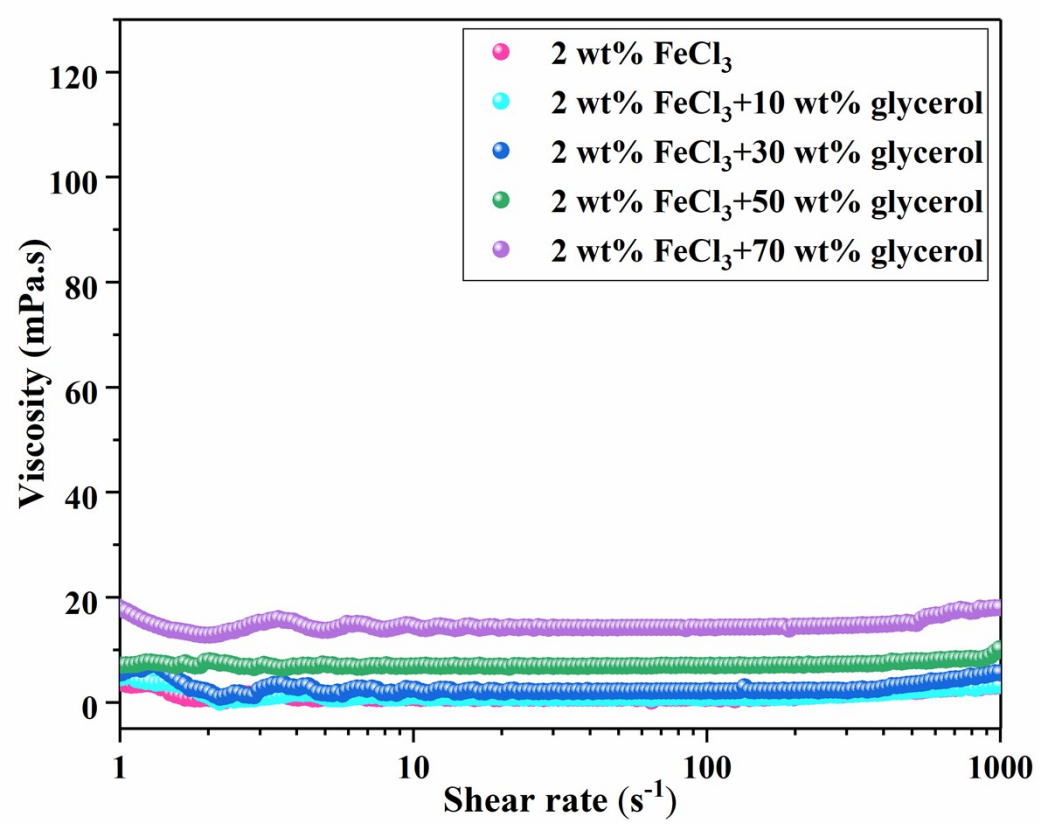

Figure S4. Shear rate-viscosity curves of five collection solutions with different viscosities.

Aqueous solution of x% $FeCl_3$ and y% glycerol	Molar Concentration of Fe^{3+}(mol/L)	Molar Concentration of glycerol(mol/L)	Calculated Osmolality(osmol/kg)
X=2, Y=0	0.123	0	0.494
X=2, Y=10	0.123	1.085894	1.581
X=2, Y=30	0.123	3.257683	3.749
X=2, Y=50	0.123	5.429471	5.920
X=2, Y=70	0.123	7.60126	8.091
X=4, Y=0	0.246609	0	0.987
X=4, Y=10	0.246609	1.085894	2.073
X=4, Y=30	0.246609	3.257683	4.245
X=4, Y=50	0.246609	5.429471	6.416
X=4, Y=70	0.246609	7.60126	8.587

X=6, Y=0	0.369914	0	1.481
X=6, Y=10	0.369914	1.085894	2.567
X=6, Y=30	0.369914	3.257683	4.741
X=6, Y=50	0.369914	5.429471	6.913
X=6, Y=70	0.369914	7.60126	9.084
X=8, Y=0	0.493218	0	1.973
X=8, Y=10	0.493218	1.085894	3.062
X=8, Y=30	0.493218	3.257683	5.230
X=8, Y=50	0.493218	5.429471	7.399
X=8, Y=70	0.493218	7.60126	9.570
X=10, Y=0	0.616523	0	2.468
X=10, Y=10	0.616523	1.085894	3.555
X=10, Y=30	0.616523	3.257683	5.726
X=10, Y=50	0.616523	5.429471	7.897
X=10, Y=70	0.616523	7.60126	10.068

Table S1. The osmotic pressure values of collection solutions composed of 2, 4, 6, 8, and 10 wt% $FeCl_3$ with 0, 10, 30, 50, and 70 wt% glycerol, respectively.

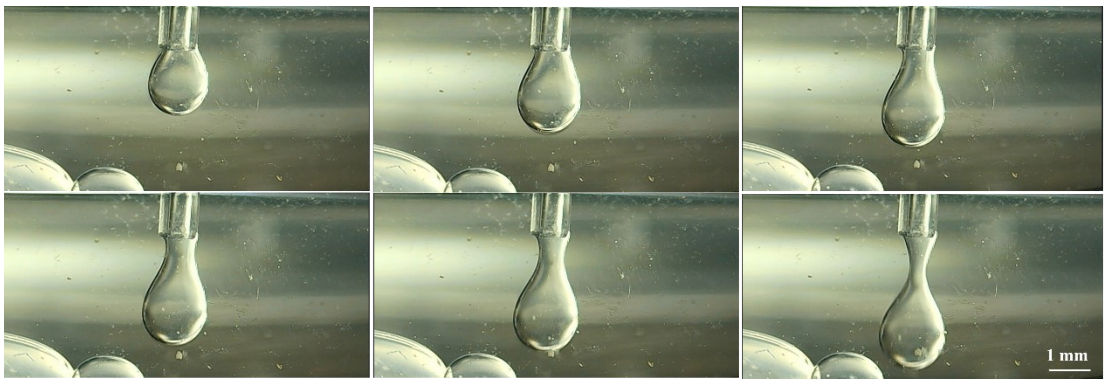

Figure S5. Photographs of the process of interfacial tension measurement

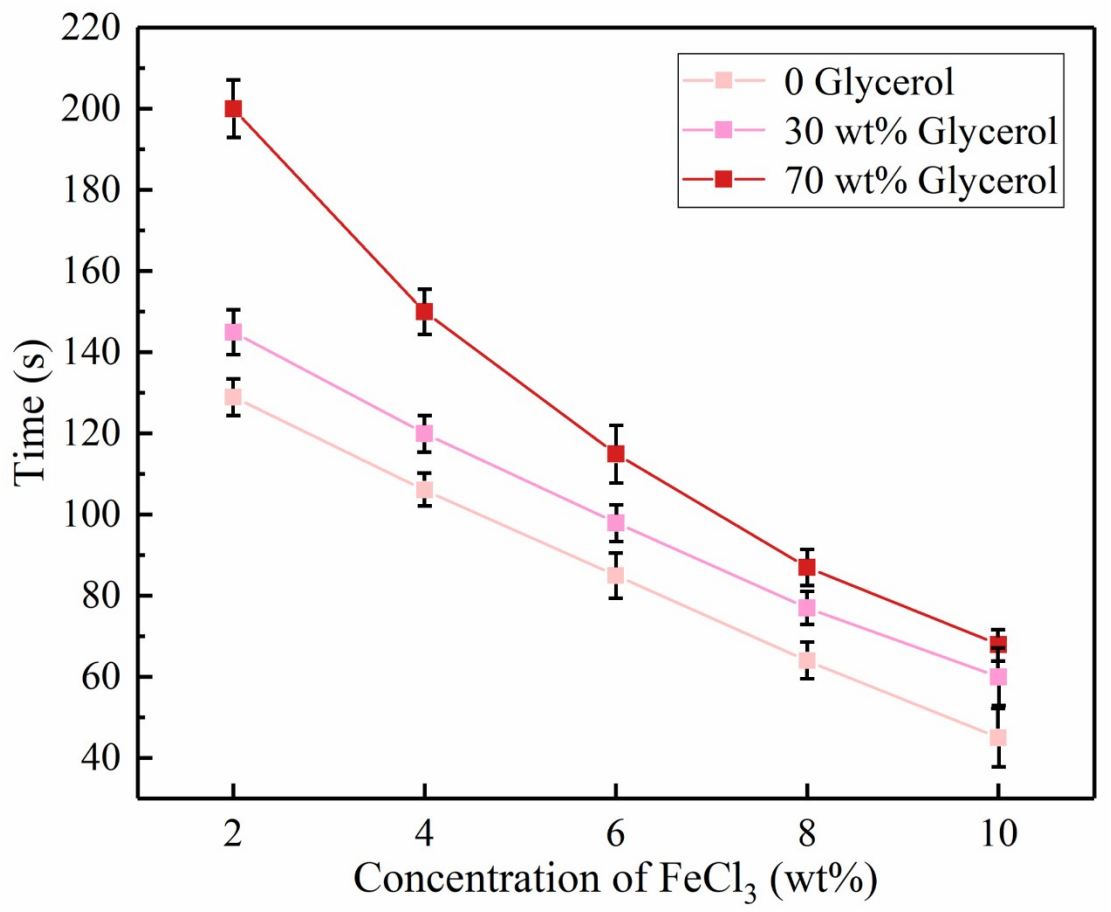

Figure S6. The cross-linking rate curves of 2 wt% SA droplets in collection solutions with different concentrations of glycerol and $FeCl_3$.

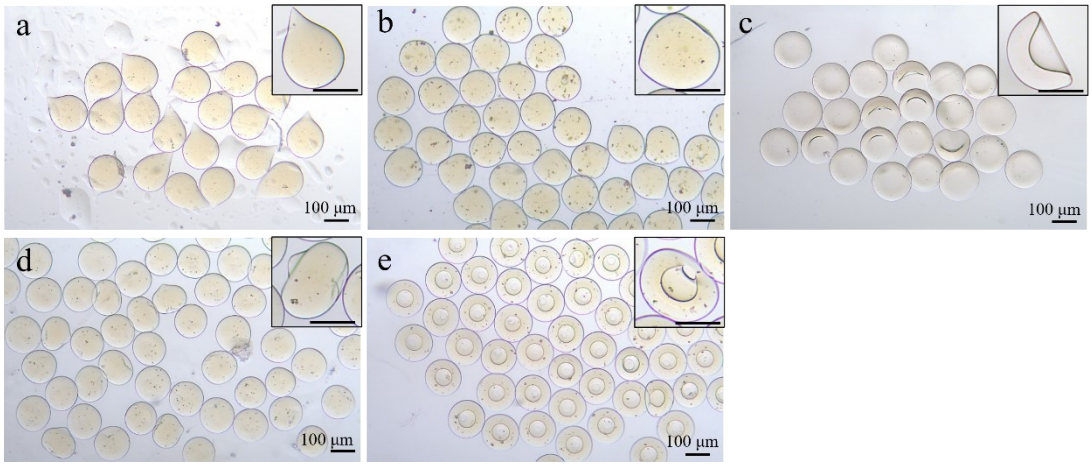

Figure S7. Optical microscopy images of five morphological types of Fe-Alginate microgels. The microgels were produced from the droplets of an aqueous solution of 2wt% SA and 10 wt% dextran. The droplets were collected in solutions with glycerol concentrations ranging from 0 to 70 wt% and $FeCl_3$ concentrations ranging from 2 to

10 wt%. The inset shows magnified side views of the microgels. a: Teardrop-like; b: peach-like; c: cap-like; d: mushroom-like; e: dimple-like with a large cavity.

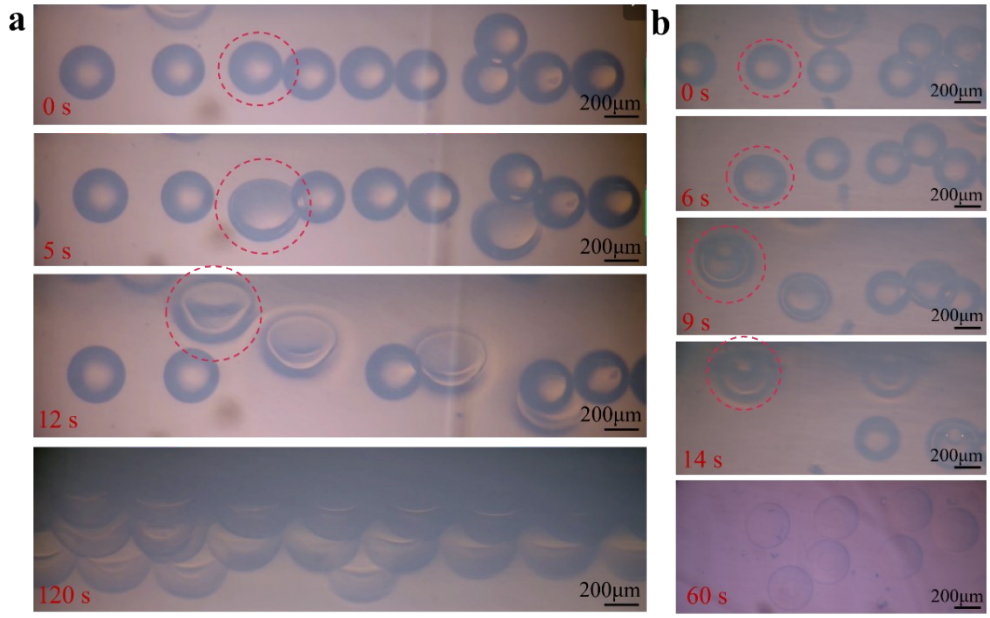

Figure S8. a. The optical microscopy images illustrate the deformation process of initial SA-Dextran droplets forming cap-like microgels in the collection solution that was composed of 2 wt% $FeCl_3$ and 70 wt% glycerol. b. The optical microscopy images illustrate the deformation process of initial SA-Dextran droplets forming dimple-like with a large cavity microgels in the collection solution that was composed of 6 wt% $FeCl_3$ and 70 wt% glycerol.

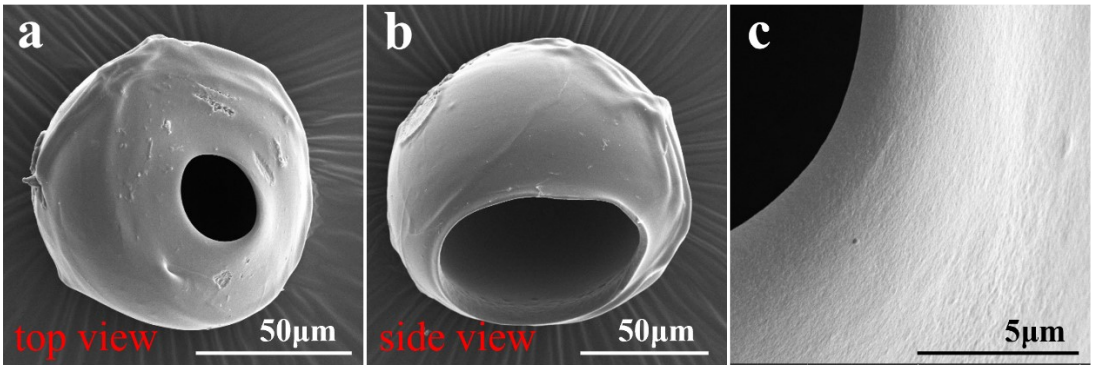

Figure S9. a-b. SEM images of dimple-like Fe-Alginate microgels formed from a SA solution containing 10 wt% Dextran as the inner phase. c. SEM image shows the surface microstructure of microgels prepared from the initial SA-Dextran droplets.

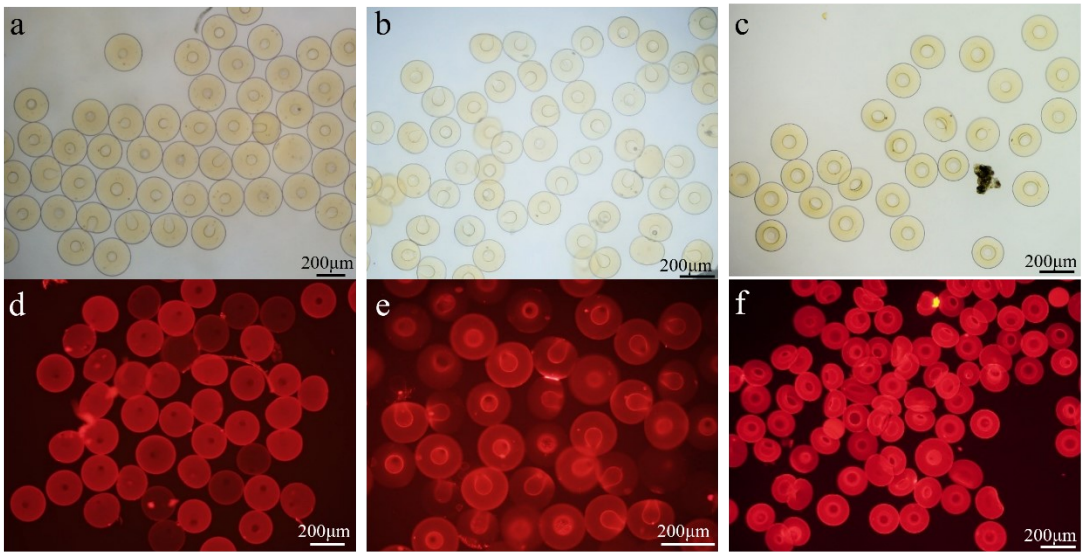

Figure S10. a-b: Optical microscopy images of dimple-like Fe-Alginate microgels with varying cavity sizes, produced from 2 wt% SA droplets containing 10 wt% dextran. d-f: Fluorescence images of three types of microgels with different cavity sizes after reacting in 0.5 wt% poly(N-isopropylacrylamide co-$Ru(bpy)_3$) solution for 30 minutes.

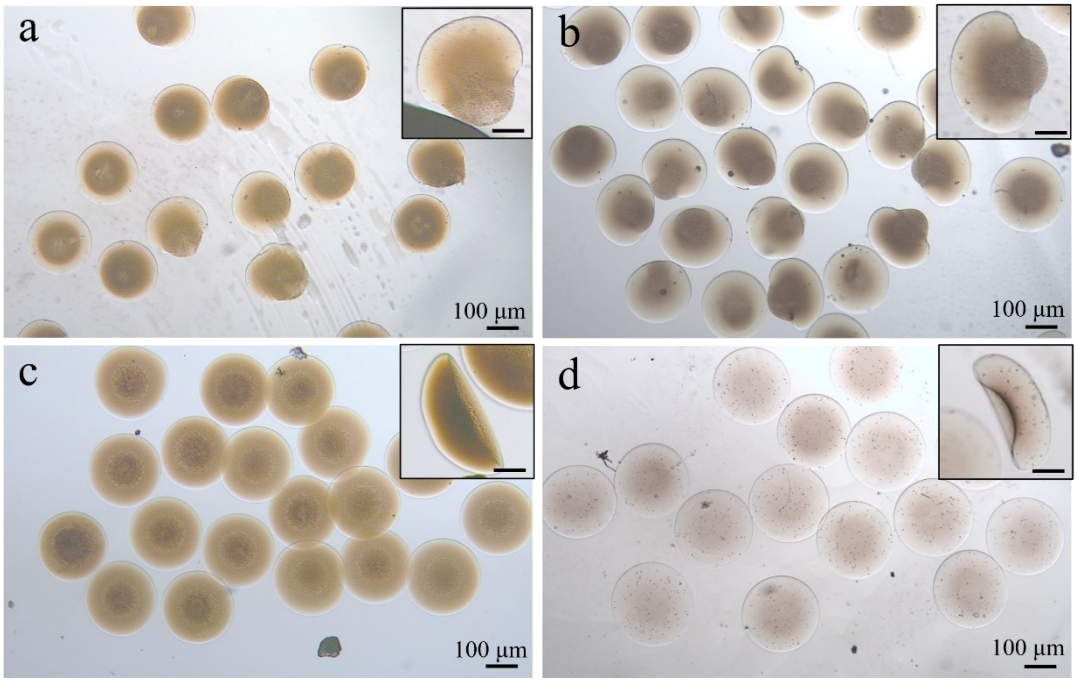

Figure S11. Optical microscopy images of four morphological types of Fe-Alginate microgels produced from droplets of 2 wt% SA and 10 wt% PEG. The droplets were collected in solutions with glycerol concentrations ranging from 0 to 70 wt% and $FeCl_3$ concentrations ranging from 2 to 10 wt%. The insets show magnified side views of the microgels. a: snowman-like; b: mushroom-like; c: convex-like; d: red blood cell-like.

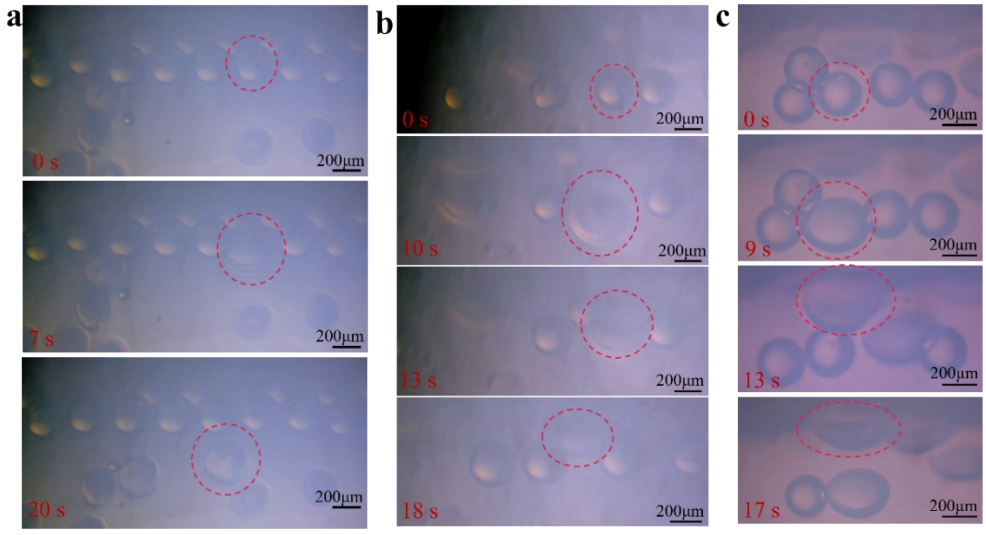

Figure S12. a. The optical microscopy images illustrate the deformation process of the initial

SA-PEG droplets forming mushroom-like microgels in the collection solution that was composed of 2 wt% $FeCl_3$ and 50 wt% glycerol. b. The optical microscopy images illustrate the deformation process of initial SA-PEG droplets forming convex-like microgels in the collection solution that was composed of 6 wt% $FeCl_3$ and 10 wt% glycerol. c. The optical microscopy images illustrate the deformation process of initial SA-PEG droplets forming red blood cell-like microgels in the collection solution that was composed of 8 wt% $FeCl_3$ and 70 wt% glycerol.

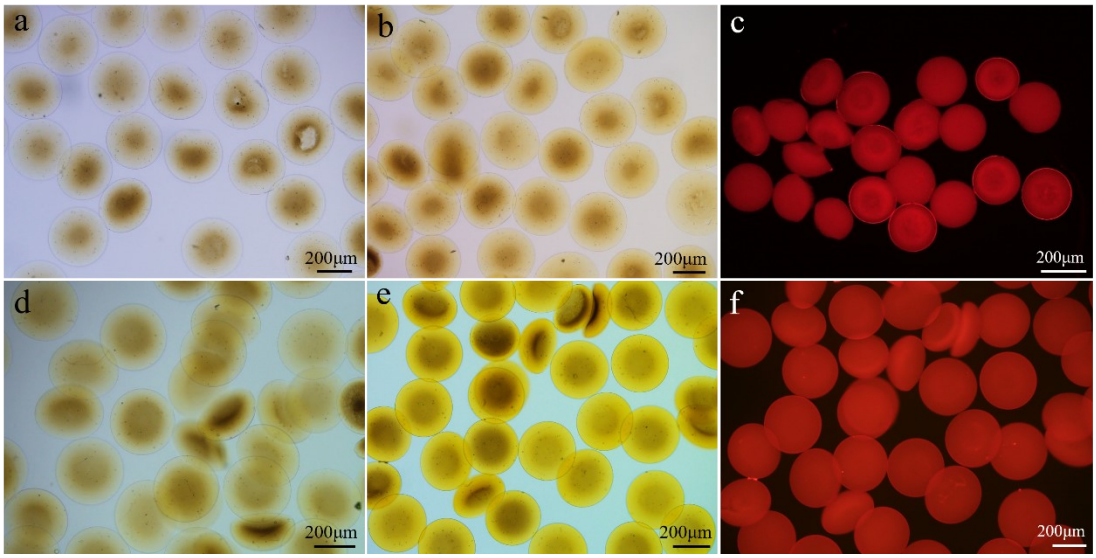

Figure S13. a-b: Optical microscopy images of convex-like Fe-Alginate microgels before and after immersion in a poly(N-isopropylacrylamide-co-$Ru(bpy)_3$) solution. c: Fluorescence image of convex-like Fe-Alginate microgels after 30 minutes of immersion in the poly(N-isopropylacrylamide-co-$Ru(bpy)_3$) solution. d-e: Optical microscopy images of red blood cell-like microgels before and after immersion in a poly(N-isopropylacrylamide-co-$Ru(bpy)_3$) solution. c: Fluorescence image of red blood

cell-like microgels after 30 minutes of immersion in the poly(N-isopropylacrylamide-co-Ru(bpy)$_3$) solution

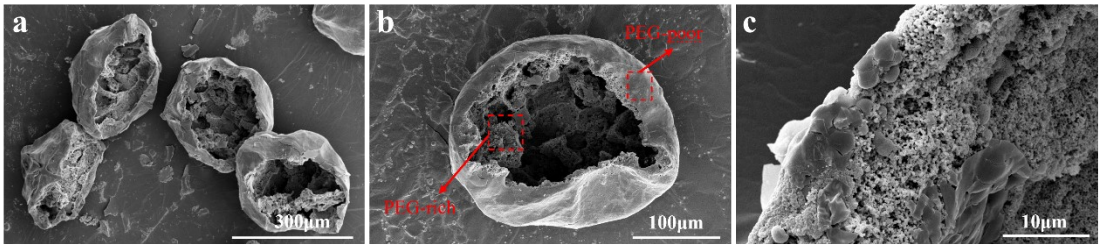

Figure S14. a-b. SEM images of red blood cell-like Fe-Alginate microgels formed from the droplets of an aqueous solution of 2 wt% SA and 10 wt% PEG. The droplets were collected in the collection solution composed of 6 wt% $FeCl_3$ and 50 wt% glycerol c. SEM micrograph of PEG-rich regions within the microgels caused by phase separation.

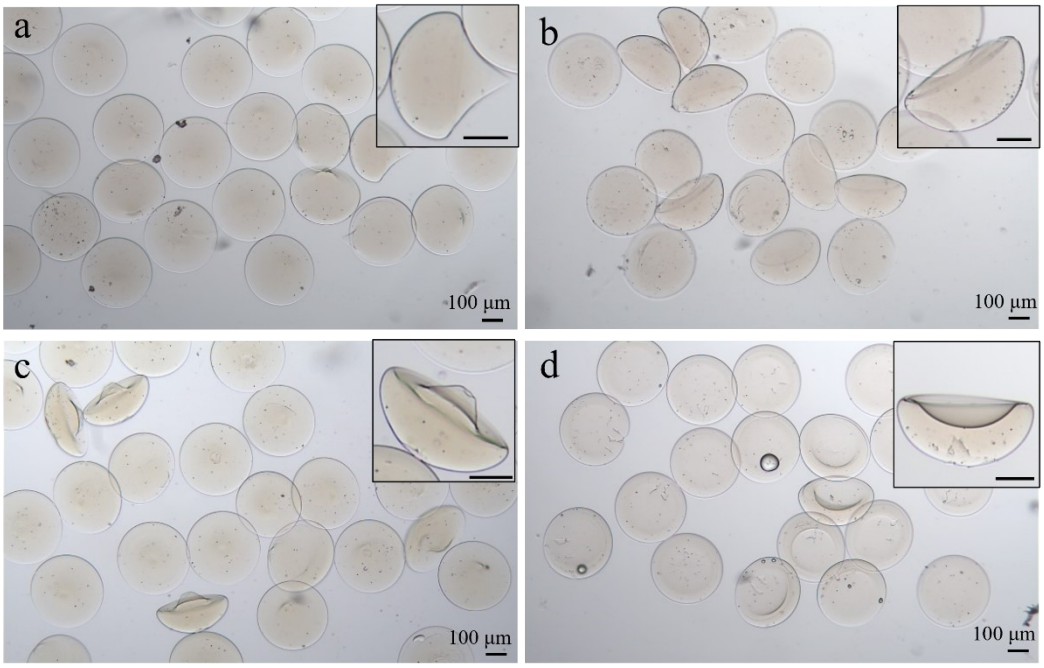

Figure S15. Optical microscopy images of four morphological types of Fe-Alginate microgels produced from droplets of an aqueous solution of 2 wt% SA and 10 wt% glycerol. The droplets were collected in solutions with glycerol concentrations ranging

from 0 to 70 wt% and $FeCl_3$ concentrations ranging from 2 to 10 wt%. The insets show the corresponding magnified side views of the microgels. a: pointed-tailed mushroom-like; b: convex-like; c: mushroom-like; d: red blood cell-like.

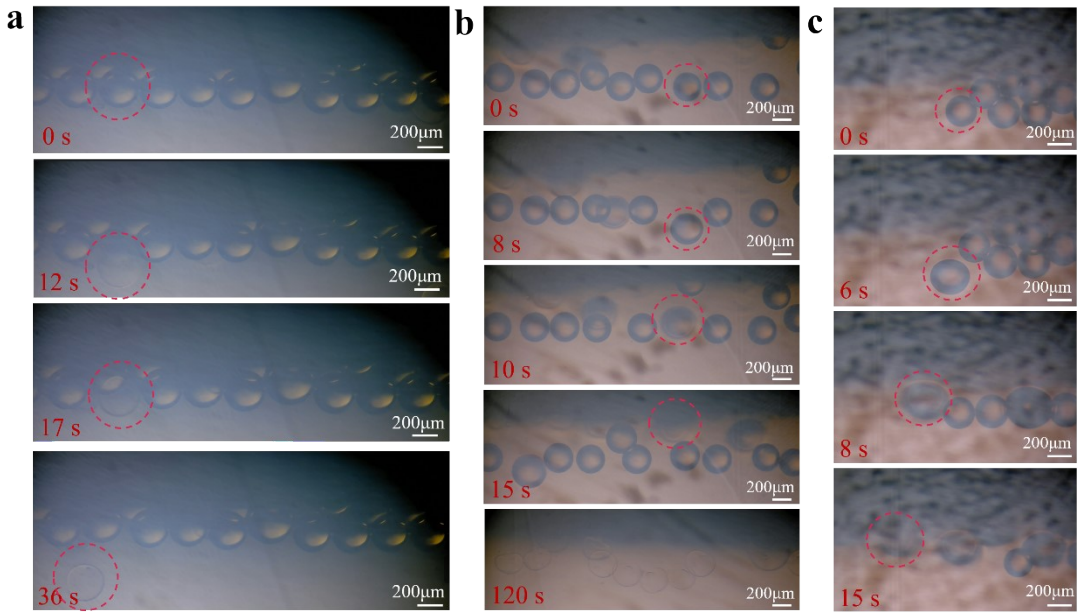

Figure S16. a. The optical microscopy images illustrate the deformation process of the initial SA-glycerol droplets forming pointed-tailed mushroom-like microgels in the collection solution composed of 2 wt% $FeCl_3$ and 30 wt% glycerol. b. The optical microscopy images illustrate the deformation process of the initial SA-glycerol droplets forming mushroom-like microgels in the collection solution composed of 4 wt% $FeCl_3$ and 30 wt% glycerol. c. The optical microscopy images illustrate the deformation process of the initial SA-glycerol droplets forming red blood cell-like microgels in the collection solution composed of 8 wt% $FeCl_3$ and 70 wt% glycerol.

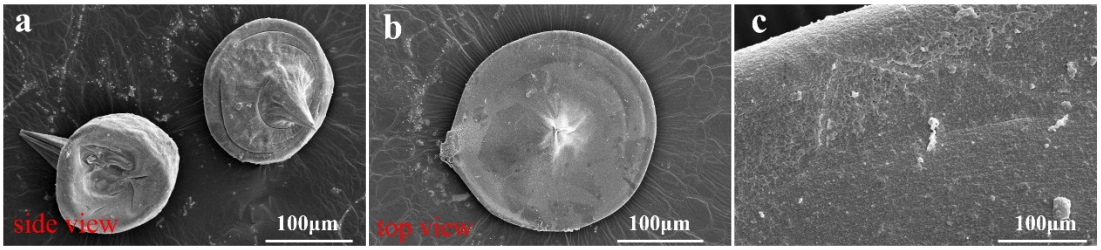

Figure S17. a-b. SEM image of Fe-Alginate microgels formed from the droplets of an aqueous solution of 2 wt% SA and 10 wt% glycerol. The droplets were collected in the collection solution composed of 2 wt% $FeCl_3$ and 30 wt% glycerol c. SEM micrograph shows the surface microstructure of microgels prepared from initial SA-glycerol droplets.

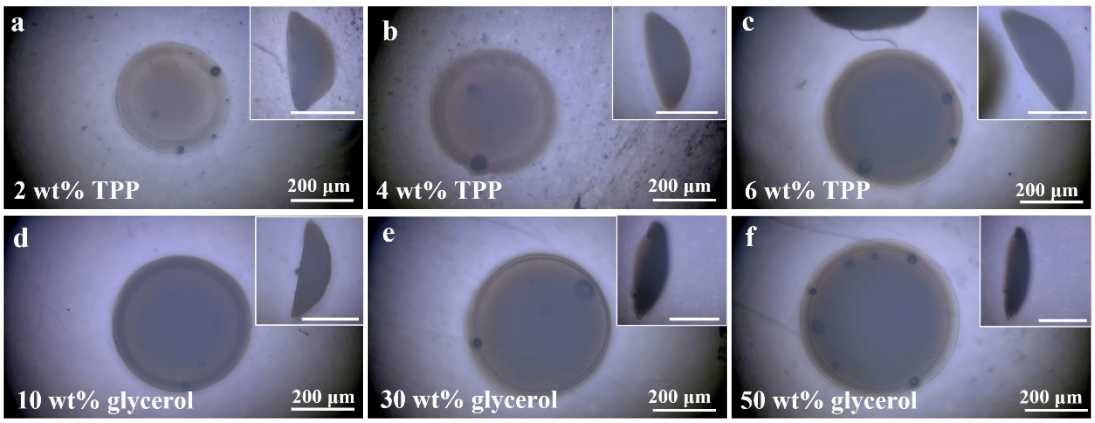

Figure S18. a-c. Optical microscopy images of CS-TPP microgels (main image: top-view; inset: side-view) in collection solutions with different TPP concentrations (2, 4, and 6 wt%) but with a fixed glycerol concentration of 10 wt%. d-f. Optical microscopy images of CS-TPP microgels obtained in collection solutions with different concentrations of glycerol (10, 30, and 50 wt%) when the TPP concentration was fixed at 6 wt%. Inset figures show the corresponding side views of the microgels.

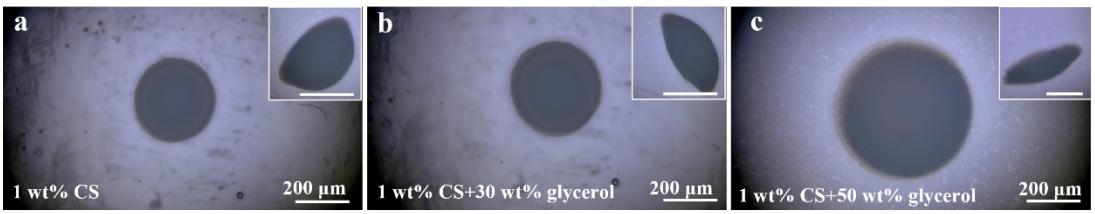

Figure S19. a-c. Optical microscopy images of CS-TPP microgels obtained by collecting 1 wt% chitosan droplets with different viscosities (by adding0, 30, and 50 wt% of glycerol into the dispersed phase, respectively) in a TPP collection solution with a fixed concentration (2 wt%). Inset figures show the corresponding side views of the microgels

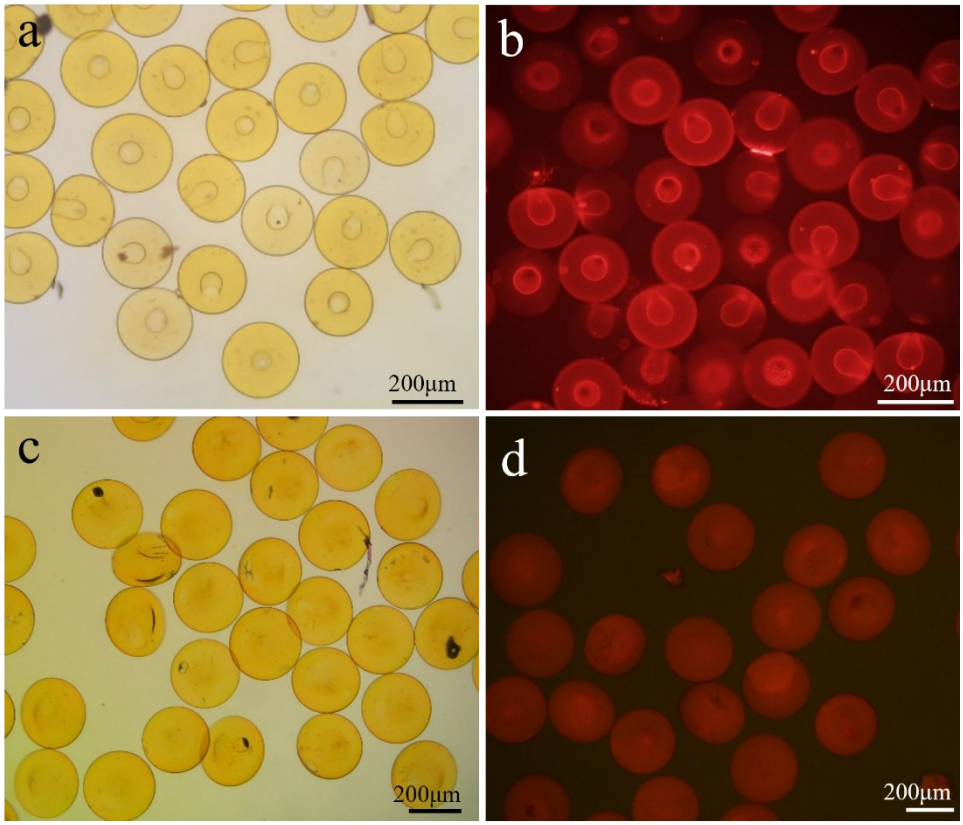

Figure S20. a-b. Optical and fluorescence microscopy images of dimpled microgels after loading of the drug molecules. c-d. Optical and fluorescence microscopy images of spherical microgels after loading of the drug molecules.

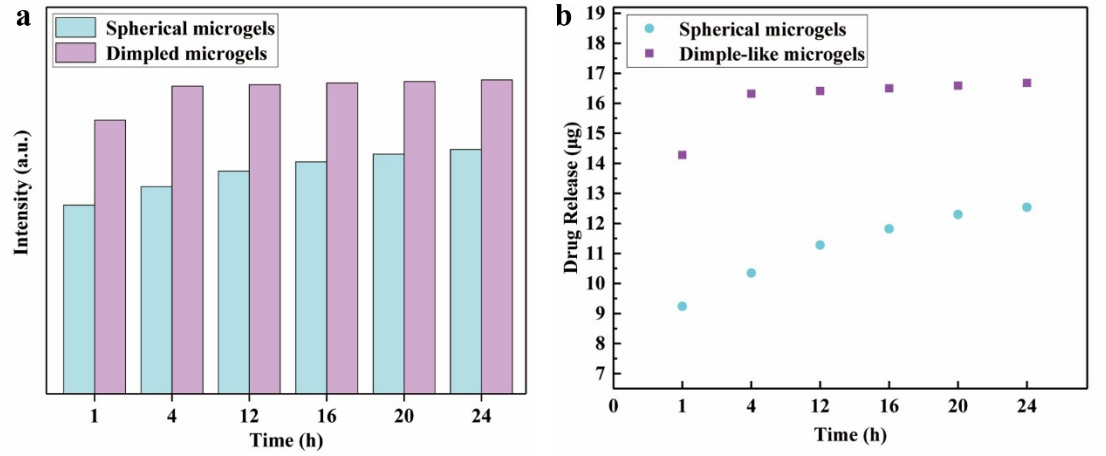

Figure S21. a. The bar chart shows the UV absorption intensity of drug release from spherical microgels and dimple-like microgels within 24 hours. b. The dynamic changes in the amount of drug released by the two types of microgels with different morphologies within 24 hours.

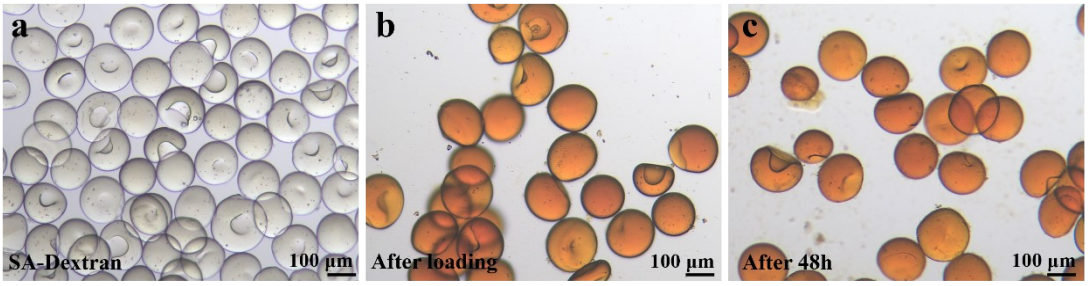

Figure S22. a. Optical microscopy image of the initial drug-free Fe-alginate microgels. b-c. Optical microscopy image of the microgels after successful drug loading by soaking in the solution of the drug model molecule for 24 hours and after drug release for 48 hours.